

Final Report

on

**Quantitative Analysis of the Detection Limits
for Heavy-Metal-Contaminated Soils by
Laser-Induced Breakdown Spectroscopy**

by

Dennis R. Alexander
Dana E. Poulain
Department of Electrical Engineering
Center for Electro-Optics
University of Nebraska-Lincoln
248 WSEC, Box 880511
Lincoln, NE 68588-0511
402-472-3091

for

Ernesto R. Cespedes
U.S. Army Corps of Engineers
Waterways Experiment Station
ATTN: CEWES-EN-B
3909 Halls Ferry Road
Vicksburg, MS 39150-6199
601-634-3906

19961016 003

Contract DACA39-95-K-0053

DTIC QUALITY INSPECTED 4

The views, opinions, and/or findings contained in this report are those of the author(s) and should not be construed as an Official Department of the Army position, policy, or decision, unless so designated by other documentation.

DISTRIBUTION STATEMENT A

**Approved for public release;
Distribution Unlimited**

REPORT DOCUMENTATION PAGE

Form Approved
OMB NO. 0704-0188

Public reporting burden for this collection of information is estimated to average 1 hour per response, including the time for reviewing instructions, searching existing data sources, gathering and maintaining the data needed, and completing and reviewing the collection of information. Send comment regarding this burden estimate or any other aspect of this collection of information, including suggestions for reducing this burden, to Washington Headquarters Services, Directorate for Information Operations and Reports, 1215 Jefferson Davis Highway, Suite 1204, Arlington, VA 22202-4302, and to the Office of Management and Budget, Paperwork Reduction Project (0704-0188), Washington, DC 20503.

1. AGENCY USE ONLY (Leave blank)		2. REPORT DATE 7/31/96		3. REPORT TYPE AND DATES COVERED 6/1/95 - 7/1/96	
4. TITLE AND SUBTITLE Quantitative Analysis of the Detection Limits for Heavy-Metal-Contaminated Soils by Laser-Induced Breakdown Spectroscopy				5. FUNDING NUMBERS Contract # DACA39-95-K-0053	
6. AUTHOR(S) Dr. Dennis R. Alexander Dr. Dana E. Poulain					
7. PERFORMING ORGANIZATION NAMES(S) AND ADDRESS(ES) Department of Electrical Engineering/Center for Electro-Optics University of Nebraska-Lincoln 248 WSEC, Box 880511 Lincoln, NE 68588-0511				8. PERFORMING ORGANIZATION REPORT NUMBER	
9. SPONSORING / MONITORING AGENCY NAME(S) AND ADDRESS(ES) U.S. Army Engineer Waterways Experiment Station 3909 Halls Ferry Road Vicksburg, MS 39180-6199				10. SPONSORING / MONITORING AGENCY REPORT NUMBER	
11. SUPPLEMENTARY NOTES The views, opinions and/or findings contained in this report are those of the author(s) and should not be construed as an official Office of Naval Research position, policy or decision, unless so designated by other documentation.					
12a. DISTRIBUTION / AVAILABILITY STATEMENT Approved for public release; distribution unlimited.				12 b. DISTRIBUTION CODE	
13. ABSTRACT (Maximum 200 words) Laser-induced breakdown spectroscopy (LIBS) is a rapid remote measurement method for detection of metals in the environment. A major factor in the quantitative use of this technique involves the minimum detection limits under laboratory and field operations. Nd:YAG laser pulses (125 mJ, $\lambda = 1.06 \mu\text{m}$) are focused on sample surfaces to produce laser sparks (plasmas). Plasma emissions are recorded after interference from broadband emissions is reduced. Results are reported on the lower detection limits of As, Cd, Cr, Hg, Pb and Zn in sand, silt, clay and kaolin. Detection limits are significantly lower in sand than silt and clay. An excimer laser (125 mJ, $\lambda = 248 \text{ nm}$) was used for comparative LIBS analysis of lead (Pb) in silt. No significant difference was found in the lower detection limits using excimer and Nd:YAG lasers. The LIBS method must provide accurate data when used in a cone penetrometer. Conditions encountered by a cone penetrometer-based LIBS system have been simulated by compressing soil samples and then allowing them to relax for specific intervals before LIBS analysis. Results are presented of the dependence of LIBS measurements on the relaxation time after soil sample compression. This data is important for a firm understanding of detection limits for field-deployable LIBS systems.					
14. SUBJECT TERMS Laser-induced breakdown spectroscopy, heavy metals, environmental monitoring				15. NUMBER OF PAGES 36	
				16. PRICE CODE	
17. SECURITY CLASSIFICATION OR REPORT UNCLASSIFIED	18. SECURITY CLASSIFICATION OF THIS PAGE UNCLASSIFIED	19. SECURITY CLASSIFICATION OF ABSTRACT UNCLASSIFIED	20. LIMITATION OF ABSTRACT UL		

TABLE OF CONTENTS

Table of Contents	ii
List of Figures	iii
List of Tables	vi
1 Summary	1
2 Introduction	2
3 Experimental Method	3
3.1 Sample Preparation	3
3.2 LIBS System	7
4 Results	9
4.1 Soil Compression Effects	9
4.2 Excitation Source	11
4.3 Calibration Data	13
4.4 Detection Limits	26
5 Conclusions	28

LIST OF FIGURES

1	Comparison of dried sand samples: (left) 50 parts-per-million (ppm) of chromium (Cr), as ammonium dichromate, and (right) doped with an equivalent volume of distilled water.	4
2	Photograph showing detail of the sand cross-section from Fig. 1, doped with 50 ppm Cr (as ammonium dichromate).	5
3	Photographs showing surface details of sand samples doped with 50 ppm Cr (as ammonium dichromate) (a) mixed once during the drying interval, and (b) mixed every 10 minutes during the drying interval.	6
4	Schematic of a typical LIBS system utilizing a Nd:YAG laser and an optical multichannel analyzer.	7
5	Effect of "relaxation time" after soil compression (20 tons for 1 minute) on LIBS measurements of 50 ppm chromium in sand.	9
6	Comparison of calibration curves for lead (Pb) in clay, based on the intensity ratio of Pb-I (405.78 nm) to Si-I (390.55 nm), obtained for Nd:YAG and excimer laser sources.	11
7	Emission spectrum showing the relevant atomic emission lines of arsenic (As) and silicon (Si) used in LIBS calibration.	14
8	Plot of the signal-noise-ratio of the As-I (278.02 nm) line to the background in the vicinity of 245 nm as a function of ICCD gate delay time.	14
9	Calibration curves for arsenic (As) in (a) sand, (b) silt, (c) clay, and (d) kaolin, based on the intensity ratio of As-I (278.02 nm) to Si-I (288.16 nm).	15

10	Emission spectrum showing the relevant atomic emission lines of cadmium (Cd) and titanium (Ti) used in LIBS calibration.	16
11	Plot of the signal-noise-ratio of the Cd-I (479.99 nm) line to the background in the vicinity of 510 nm as a function of ICCD gate delay time.	16
12	Calibration curves for cadmium (Cd) in (a) sand, (b) silt, (c) clay, and (d) kaolin, based on the intensity ratio of Cd-I (479.99 nm) to Ti-I (498.17 nm).	17
13	Emission spectrum showing the relevant atomic emission lines of chromium (Cr) and silicon (Si) used in LIBS calibration.	18
14	Plot of the signal-noise-ratio of the Cr-I (425.44 nm) line to the background in the vicinity of 417 nm as a function of ICCD gate delay time.	18
15	Calibration curves for chromium (Cr) in (a) sand, (b) silt, (c) clay, and (d) kaolin, based on the intensity ratio of Cr-I (425.44 nm) to Si-I (390.55 nm).	19
16	Emission spectrum showing the relevant atomic emission lines of mercury (Hg) and titanium (Ti) used in LIBS calibration.	20
17	Plot of the signal-noise-ratio of the Hg-I (435.83 nm) line to the background in the vicinity of 460 nm as a function of ICCD gate delay time.	20
18	Calibration curves for mercury (Hg) in (a) sand, (b) silt, (c) clay, and (d) kaolin, based on the intensity ratio of Hg-I (435.83 nm) to Ti-I (498.17 nm).	21
19	Emission spectrum showing the relevant atomic emission lines of lead (Pb) and silicon (Si) used in LIBS calibration.	22
20	Plot of the signal-noise-ratio of the Pb-I (405.78 nm) line to the background in the vicinity of 409 nm as a function of ICCD gate delay time.	22
21	Calibration curves for lead (Pb) in (a) sand, (b) silt, (c) clay, and (d) kaolin, based on the intensity ratio of Pb-I (405.78 nm) to Si-I (390.55 nm).	23
22	Emission spectrum showing the relevant atomic emission lines of zinc (Zn) and titanium (Ti) used in LIBS calibration.	24
23	Plot of the signal-noise-ratio of the Zn-I (481.05 nm) line to the background in the vicinity of 479 nm as a function of ICCD gate delay time.	24

- 24 Calibration curves for zinc (Zn) in (a) sand, (b) silt, (c) clay, and (d) kaolin,
based on the intensity ratio of Zn-I (481.05 nm) to Ti-I (498.17 nm). 25

LIST OF TABLES

1	Summary of soil matrices used in detection limit analysis.	3
2	Summary of solutions used for doping soil matrices used in detection limit analysis.	4
3	Relevant instrument parameters for LIBS calibrations.	13
4	Lower detection limits for As, Cd, Cr, Hg, Pb and Zn in sand, silt, clay and kaolin samples.	26

1 Summary

Laser-induced breakdown spectroscopy (LIBS) is a rapid remote measurement method for detection of metals in the environment. A major factor in the quantitative use of this technique involves the minimum detection limits under both laboratory and field operations. Research on limits of detection of heavy metals in different types of soils under various conditions using LIBS has been carried out under Contract DACA39-95-K-0053. Pulses from a Nd:YAG laser operating at 125 mJ at $\lambda = 1.06 \mu\text{m}$ are focused on sample surfaces to produce laser sparks (plasmas). Atomic emissions from the plasmas are recorded using an optical multichannel analyzer after delays of a few microseconds when interference from broadband emissions is reduced.

Research has been performed on the detection limits of As, Cd, Cr, Hg, Pb and Zn in soil matrices. Results are reported on the lower detection limits of these six elements in sand, silt, clay and kaolin matrices. Detection limits are significantly lower for heavy metals in sand matrices than silt and clay matrices due to differences between surface and volume contamination.

An excimer laser operating at 125 mJ at $\lambda = 248 \text{ nm}$ was used to provide a comparative LIBS analysis for lead (Pb) in a silt matrix. No significant difference in the lower detection limit was obtained by using an excimer laser as the excitation source in place of the Nd:YAG laser.

The LIBS method must provide accurate data when used in a cone penetrometer. Conditions that would be encountered by a cone penetrometer-based LIBS system have been simulated by compressing soil samples and then allowing them to relax for specific intervals before LIBS analysis. Results are presented of the dependence of LIBS measurements on the relaxation time after soil sample compression. This data is important in order to have a firm understanding of lower detection limits for field-deployable LIBS systems.

2 Introduction

Recently interest in sensors to accurately assess and monitor the extent of environmental contamination around waste disposal sites and research facilities has grown markedly. There is an ever-increasing need to quickly and accurately perform concentration measurements of chemical species *in situ*. Previously these measurements could only be performed in the laboratory. However, the volume of measurements to be performed today and in the future have a prohibitive cost of time and finances to acquire soil or water samples and return them to a laboratory for analysis. Thus, new methods are needed to perform remote measurements quickly and efficiently, while maintaining comparable analysis capabilities.

LIBS is one method with the potential to satisfy these requirements. In this method the laser source serves to vaporize, atomize, and excite the sample material in the course of one laser pulse. This method, termed laser-induced breakdown spectroscopy (LIBS), has been used in analyses of gases,¹ liquids,^{2,3} solids,⁴ solid aerosols,⁵⁻⁷ liquid aerosols,⁸⁻¹⁰ and soils.¹¹⁻¹⁴ Because of the relative simplicity of LIBS, it is well-suited for use in the field. One existing field-deployable site characterization system to which LIBS could be adapted is the Site Characterization and Cone Penetrometer System (SCAPS) developed by the Army Corps of Engineers' Waterways Experiment Station (WES). SCAPS sensors, housed in a cone penetrometer, are driven into the soil by a hydraulic ram to depths of up to 200 feet. Measurements are performed *in situ* during the descent and/or ascent of the penetrometer. Thus, there is the potential to determine contaminant plume boundaries on-site.

As part of an on-going effort to develop LIBS for use with SCAPS, the current work reports lower detection limits for arsenic (As), cadmium (Cd), chromium (Cr), mercury (Hg), lead (Pb) and zinc (Zn) in sand, silt, clay and kaolin matrices. Also, several influences on LIBS concentration measurements of these heavy metals in the various matrices are discussed.

3 Experimental Method

3.1 Sample Preparation

Four soil or soil-like matrices were considered in this investigation: sand, silt, clay and kaolin. The materials and corresponding suppliers are noted in Table 1. Washed and dried sand

Table 1: Summary of soil matrices used in detection limit analysis.

Soil Type	Supplier
sand	Mallinckrodt Chemical, Inc., No. 7062
silt	USACE-WES
clay	USACE-WES
kaolin	Mallinckrodt Chemical, Inc., No. 5645

(Mallinckrodt Chemical, Inc., No. 7062 KPTN) was used in place of "Yuma" sand (obtained from USACE-WES) because the sand was found to already contain up to 4 ppm chromium. Silt, obtained from USACE-WES, was used as supplied. Clay, also obtained from USACE-WES, was sifted through a 1 mm mesh to remove large granular materials prior to doping with heavy metals. Kaolin (Mallinckrodt Chemical, Inc., No. 5645) is the principal component of kaolinite clay. It is a hydrous silicate of aluminum. Kaolin was used in this work because it approximates a relatively "pure" clay.

Contamination of the soil matrices was accomplished by doping the samples with solutions of the heavy metals at various concentrations to achieve the desired parts-per-million (by mass) of the metals to the soils. The compounds used to produce the solutions of the six heavy metals are noted in Table 2. The compounds were each dissolved in distilled water to produce a primary solution. For each soil sample, solutions were prepared such that addition of 10 milliliters of the solution to 50 grams of soil would result in a concentration of heavy metal in the soil between 100 parts-per-billion (ppb) and 2,000 parts-per-million (ppm). Diluted solutions were derived from the primary solutions by dilution with distilled water.

Table 2: Summary of solutions used for doping soil matrices used in detection limit analysis.

Element	Source Chemical
As	arsenic trioxide (As_2O_3)
Cd	cadmium chloride ($CdCl_2 \cdot 2\frac{1}{2}H_2O$)
Cr	ammonium dichromate ($(NH_4)_2Cr_2O_7$)
Hg	mercuric chloride ($HgCl_2$)
Pb	lead nitrate ($Pb(NO_3)_2$)
Zn	zinc chloride ($ZnCl_2$)

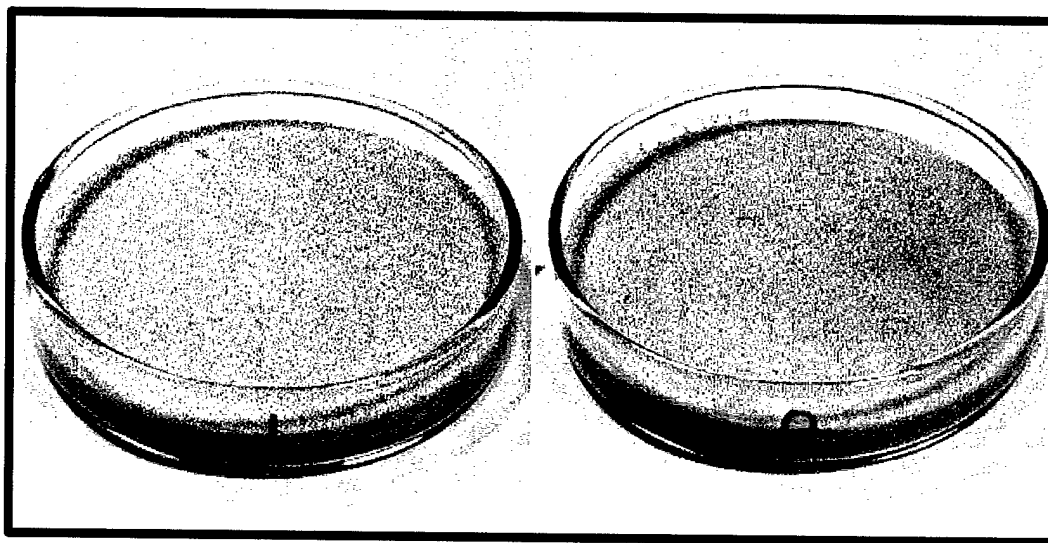


Figure 1: Comparison of dried sand samples: (left) 50 parts-per-million (ppm) of chromium (Cr), as ammonium dichromate, and (right) doped with an equivalent volume of distilled water.

An important consideration in the sample preparation process became evident during preparation of the chromium samples. Due to the strong yellow-orange color of the ammonium dichromate solution, inhomogeneities of the sample were plainly visible at higher doping concentrations (approximately 5 ppm and greater). Shown in Fig. 1 are petri dishes containing sand samples with 50 ppm Cr (left) and 0 ppm Cr (right). The sample with 50 ppm Cr has a noticeably more intense color on the surface of the sample. A detailed view of the sample

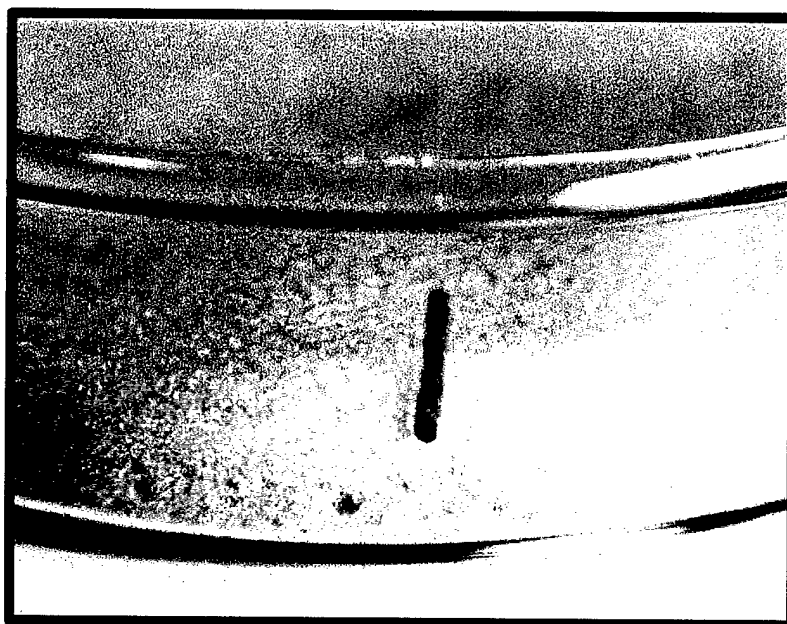
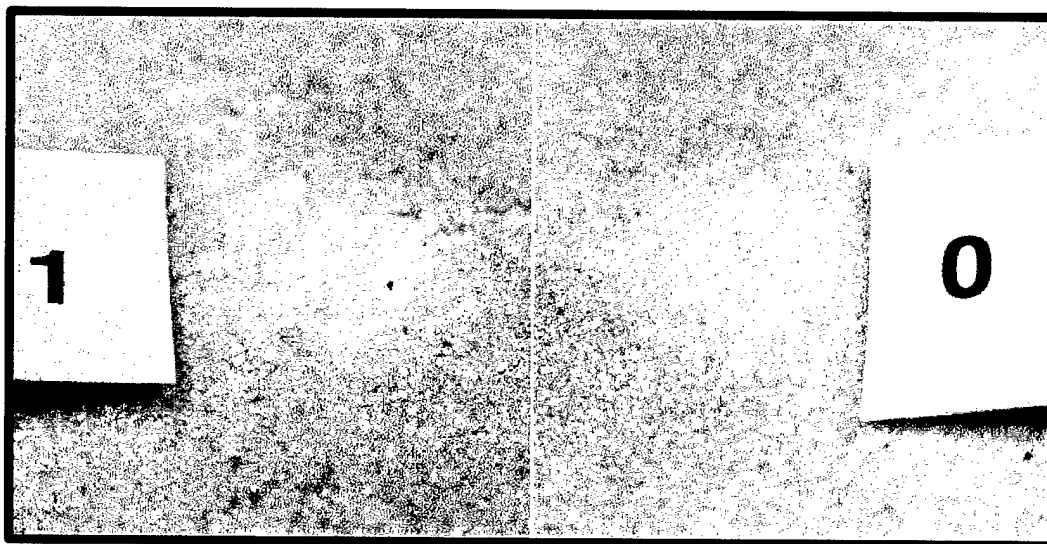


Figure 2: Photograph showing detail of the sand cross-section from Fig. 1, doped with 50 ppm Cr (as ammonium dichromate).

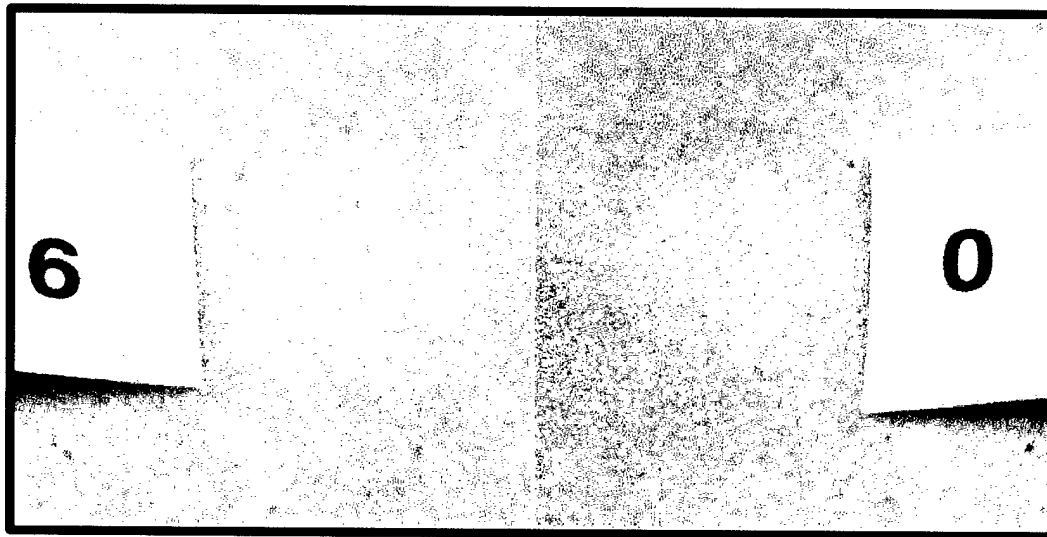
through the wall of the petri dish is shown in Fig. 2. In this figure, it is observed that the chromium appears to be concentrated in the top 1 mm of the sample.

Shown in Fig. 3 are the results of various mixing methods on two chromium doped sand samples (with a non-doped sand sample for comparison). The photograph in Fig. 3(a) is a detail of the surface of a sand sample, doped with 50 ppm Cr, mixed once during the drying interval and then mixed just prior to photographing. The photograph in Fig. 3(b) is a detail of the surface of a sand sample, also doped with 50 ppm Cr, but mixed every 10 minutes during the drying interval. Evident in Fig. 3(a) are the localized regions of high chromium concentration. In the context of LIBS calibration, detection limits decrease as the standard deviation of the emission intensity ratios decrease. Comparison of Fig. 3(a)(left) and Fig. 3(b)(left) suggests that mixing of the sample only after drying does not distribute the dopant material in the most uniform manner throughout the soil.

Samples in the investigation of compression effects were prepared by placing contaminated soils into aluminum sample holders (wall thickness approx. 0.25 in.) and loading with 20 tons force in an hydraulic press for a period of 1 minute.



(a) Sand (50 ppm Cr) mixed once during drying (left) compared to reference sand (0 ppm Cr) (right)



(b) Sand (50 ppm Cr) mixed every 10 minutes during drying (left) compared to reference sand (0 ppm Cr) (right)

Figure 3: Photographs showing surface details of sand samples doped with 50 ppm Cr (as ammonium dichromate) (a) mixed once during the drying interval, and (b) mixed every 10 minutes during the drying interval.

3.2 LIBS System

A schematic of the experimental arrangement used in performing the experimental research is shown in Fig. 4. A pulsed Nd:YAG laser (Big Sky Laser, Model 100R), operating at the

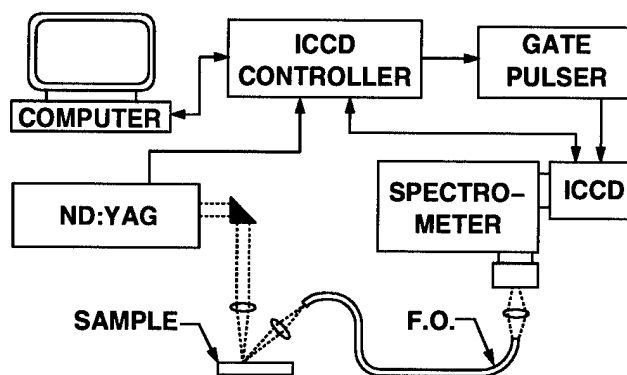


Figure 4: Schematic of a typical LIBS system utilizing a Nd:YAG laser and an optical multi-channel analyzer.

principal wavelength ($\lambda = 1.06 \mu\text{m}$) and 10 ns pulse width, serves as the excitation source. The laser radiation is focused by a plano-convex BK7 lens (diameter (ϕ) = 15 mm, focal length (f) = 100 mm) on the soil sample. An optical multi-channel analyzer (OMA), consisting of a spectrometer (Instruments SA, Model HR-320, $f = 320 \text{ mm}$) equipped with an intensified CCD camera (ICCD)(Princeton Instruments, Model ICCD-1024MG-E), is used to analyze the spectra of the plasma emissions. Emission from the laser-produced plasma is focused by a fused silica lens into an optical fiber (3M, TECS FT-1.0-UMT) for transmission to the OMA. Transmitted light from the fiber is coupled into the OMA with a bi-convex fused silica lens ($\phi = 25 \text{ mm}$, $f = 50 \text{ mm}$). An aperture between the lens and OMA slit matches the $F/\#$ of the lens to the spectrometer. The entrance slit of the spectrometer is typically opened $25 \mu\text{m}$. The region of the plasma imaged by the spectrometer is approximately 1 mm in diameter. The spectrometer is equipped with a 1200 lines/mm holographically ruled diffraction grating. The OMA was able to acquire individual spectra from the LIB plasma at the rate of approximately two per second. To increase the signal-to-noise ratio for the atomic emission lines, and thus reduce the limits of detection, the ICCD is gated. A Q-switch sync signal from the Nd:YAG triggers a gate pulse generator (Princeton Instruments, Model PG-200). The gate pulse generator triggers the OMA

and provides for delay of the gate pulse after the laser pulse and variation of the gate pulse width (integration time).

4 Results

4.1 Soil Compression Effects

A cone penetrometer inherently requires large forces to be applied to the soil in the immediate vicinity of the tip. To understand the effect of soil compression on LIBS measurements, soil samples contaminated with chromium were compressed then allowed to relax for various periods before LIBS analysis. Sand samples (~ 75 g) were doped with 50 ppm Cr (w/w). Samples were then compressed in aluminum sample holders under a load of 20 tons for one minute. Different samples were allowed to relax from 2 to 20 minutes before being analyzed using LIBS. Data for less than two minutes was not possible due to sample preparation location and the time required to perform the first LIBS measurements. Results of two trials are shown in Fig. 5. The emission intensity ratio of Cr-I (425.44 nm) to Si-I (390.55 nm) increases during the first 6

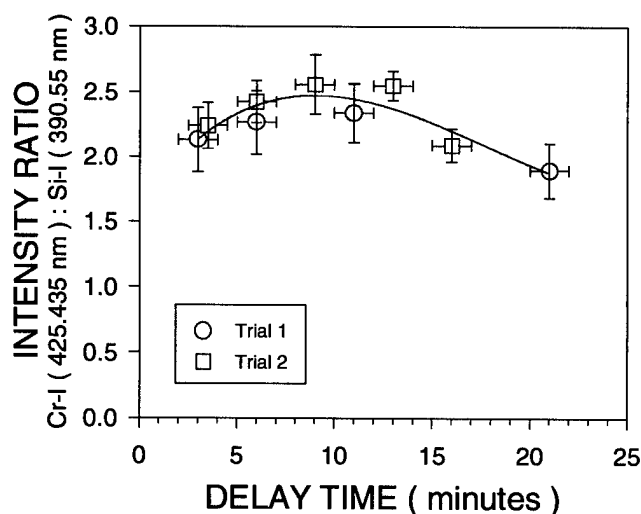


Figure 5: Effect of “relaxation time” after soil compression (20 tons for 1 minute) on LIBS measurements of 50 ppm chromium in sand.

to 10 minutes before decreasing to a level approximately equal to the initial measurement. The notation, Cr-I (425.44 nm), refers to the singly ionized chromium emission line at 425.44 nm wavelength. This notation is used throughout this report for other elements and their ionization emission.

We believe that two competing processes are responsible for the observed time-dependence of the measurements. One effect is related to the soil moisture content which is known to

decrease the intensity ratio as the moisture content increases. As the soil moisture increases a greater portion of the laser pulse is required to excite water adsorbed on the sand granules. As the soil is compressed, moisture is expelled from the soil matrix. During the relaxation period humidity from the ambient air is readsorbed by the sand. A second contributing effect is due to energy being stored in the sand particles by the compression process. Since the energy introduced by the compression process is stored mainly in the silicon (silicon dioxide) there will be a trend for the silicon line intensity to increase over the chromium line intensity. In addition, any stored energy makes it easier to produce a slightly higher plasma temperature. The stored energy effect is not permanent and relaxes in time (~ 20 minutes).

4.2 Excitation Source

The relative importance of excitation laser wavelength used in the LIBS analysis was investigated by comparison of LIBS calibration data for lead (Pb) in a silt matrix. Samples with concentrations of Pb ranging from 100 to 2000 ppm in silt were analyzed by LIBS with excimer ($\lambda = 248$ nm) and Nd:YAG ($\lambda = 1064$ nm) lasers. The resulting calibration information is shown in Fig. 6. Lower detection limits were determined according to the relation $C_L = 2S/M$,

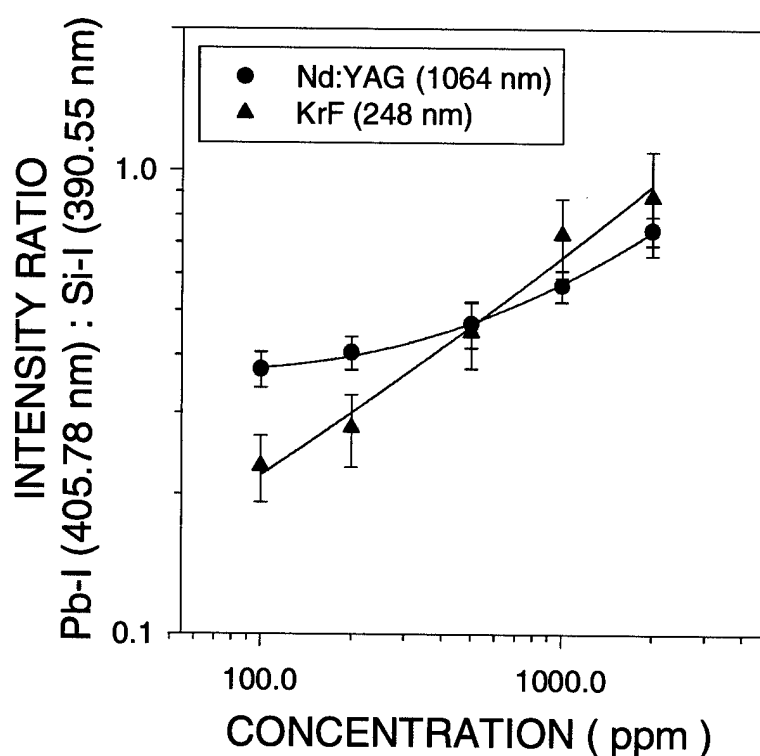


Figure 6: Comparison of calibration curves for lead (Pb) in clay, based on the intensity ratio of Pb-I (405.78 nm) to Si-I (390.55 nm), obtained for Nd:YAG and excimer laser sources.

where C_L is the lower detection limit, S is the sample standard deviation and M is the slope of the calibration curve near the lower limit. Using this method, the values of C_L for the excimer and Nd:YAG lasers were 180 and 210 ppm, respectively. The slope of the calibration curve is greater for the excimer laser, suggesting a lower detection limit, but is offset by a greater standard deviation. This increased sample standard deviation is attributed to the relative instability of the excimer laser as compared to the Nd:YAG. Thus, no significant increase in

detection limit can be expected by using an excimer laser instead of a Nd:YAG laser, even though the excimer produced lines are generally better resolved.

4.3 Calibration Data

Calibration curves were developed for each of the heavy metals in sand, silt, clay and kaolin with the following relevant instrument parameters.

Table 3: Relevant instrument parameters for LIBS calibrations.

Parameter	Value
Ambient temperature	22-24 °C
Ambient relative humidity	50-60%
Laser pulse energy	125 mJ
Laser repetition rate	4 Hz
OMA slit width	10-20 μm
OMA grating (As,Cr,Pb)	600 g/mm, $\lambda_{\text{blaze}} = 300 \text{ nm}$
OMA grating (Cd,Hg,Zn)	600 g/mm, $\lambda_{\text{blaze}} = 450 \text{ nm}$
ICCD gate delay	2-5 μs
ICCD gate width	200 μs
ICCD gain	8.0
ICCD temperature	-40 °C

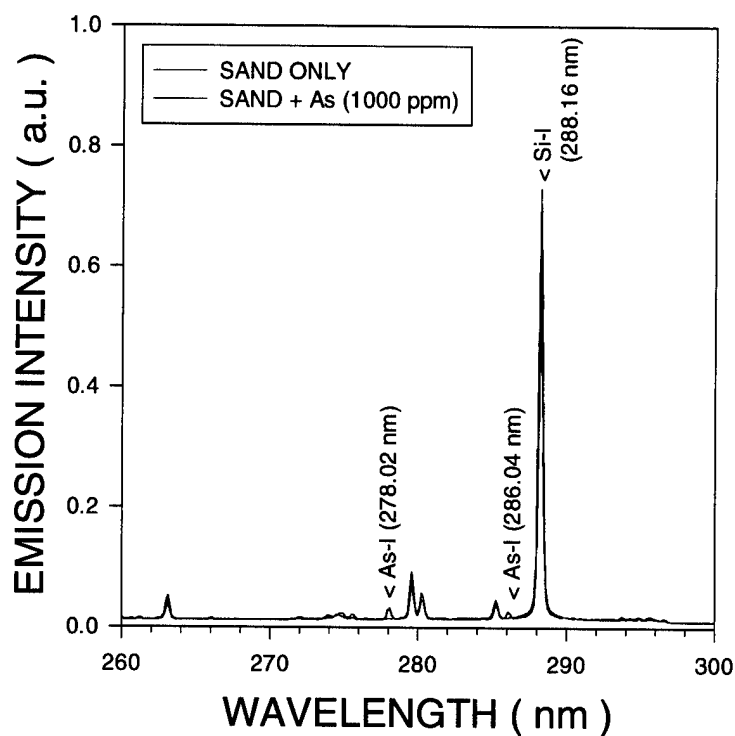


Figure 7: Emission spectrum showing the relevant atomic emission lines of arsenic (As) and silicon (Si) used in LIBS calibration.

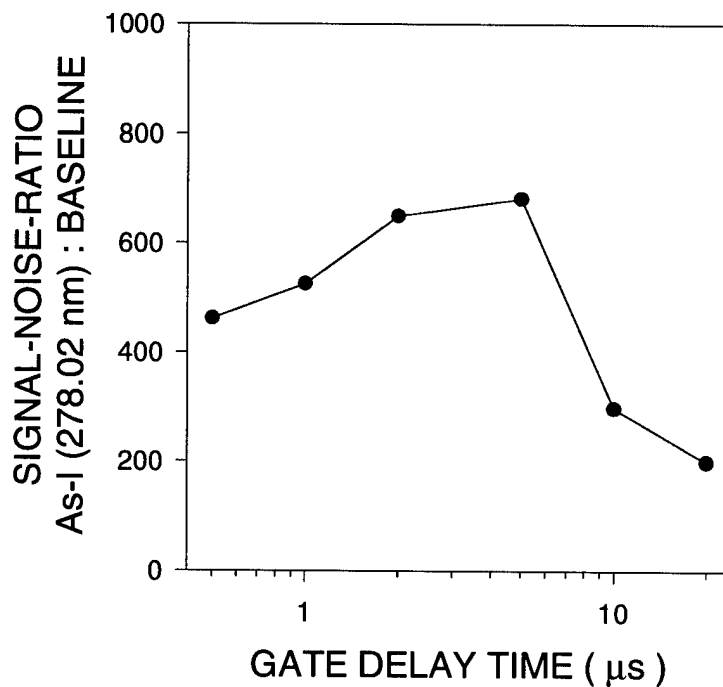


Figure 8: Plot of the signal-noise-ratio of the As-I (278.02 nm) line to the background in the vicinity of 245 nm as a function of ICCD gate delay time.

Arsenic (As)

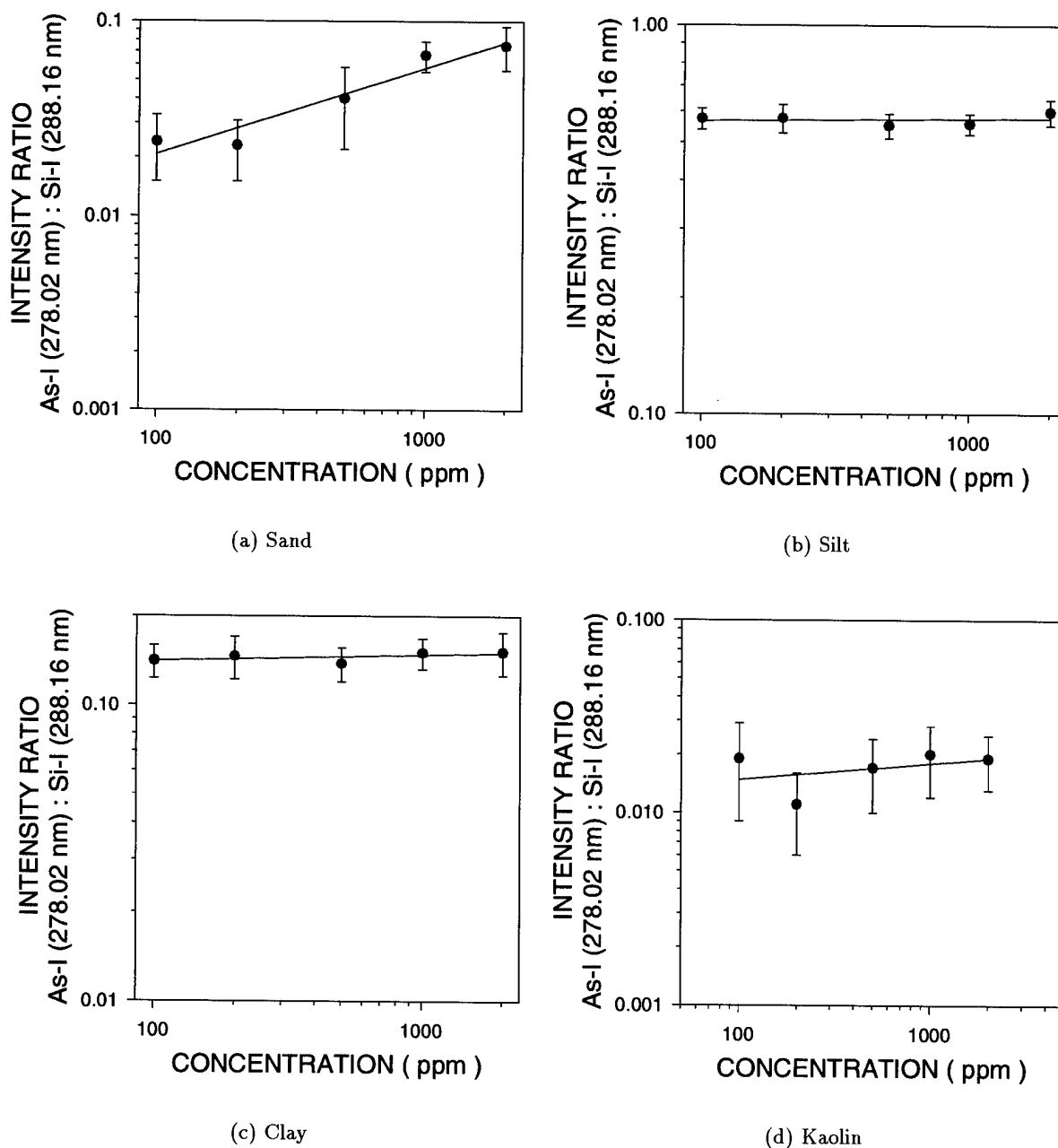


Figure 9: Calibration curves for arsenic (As) in (a) sand, (b) silt, (c) clay, and (d) kaolin, based on the intensity ratio of As-I (278.02 nm) to Si-I (288.16 nm).

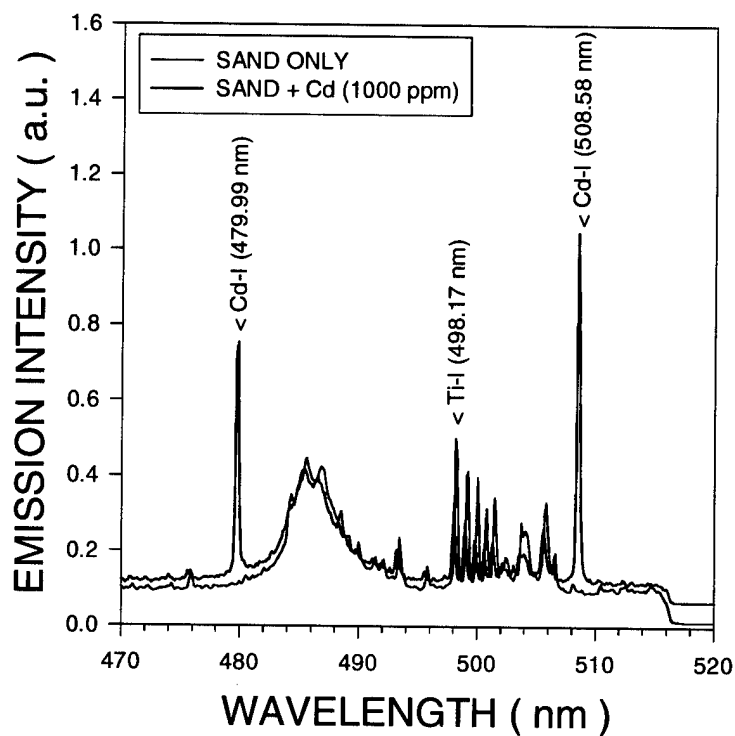


Figure 10: Emission spectrum showing the relevant atomic emission lines of cadmium (Cd) and titanium (Ti) used in LIBS calibration.

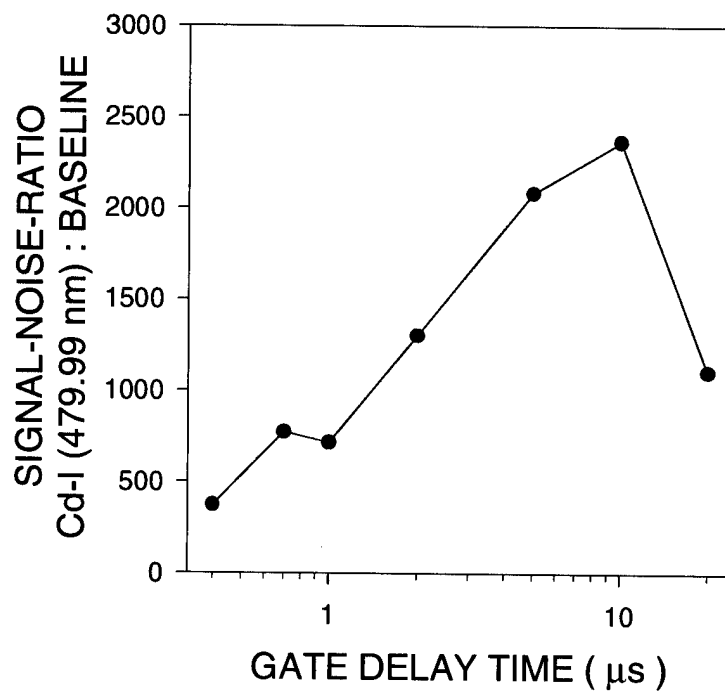
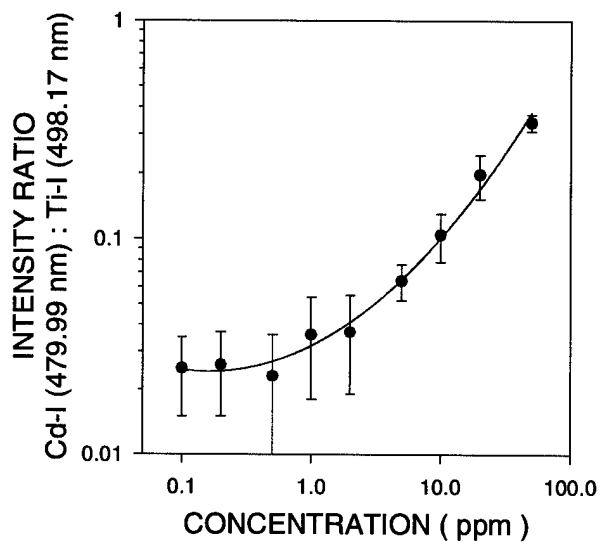
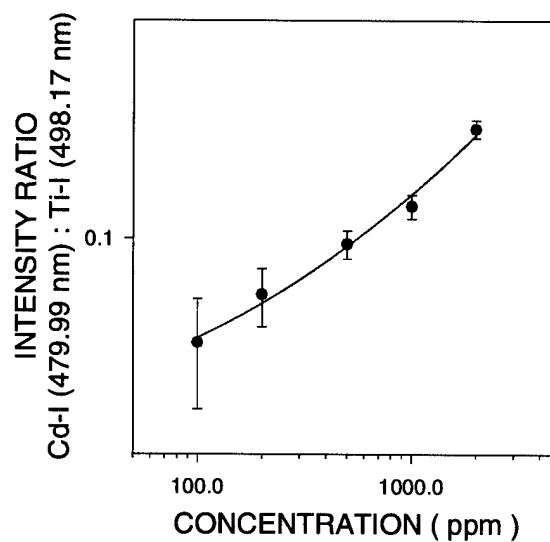


Figure 11: Plot of the signal-noise-ratio of the Cd-I (479.99 nm) line to the background in the vicinity of 510 nm as a function of ICCD gate delay time.

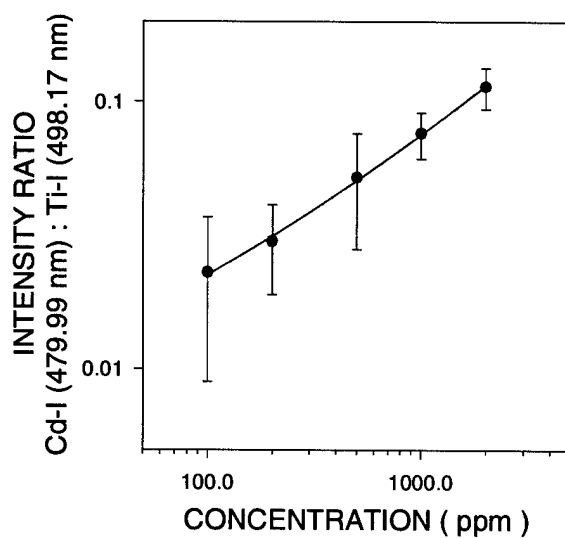
Cadmium (Cd)



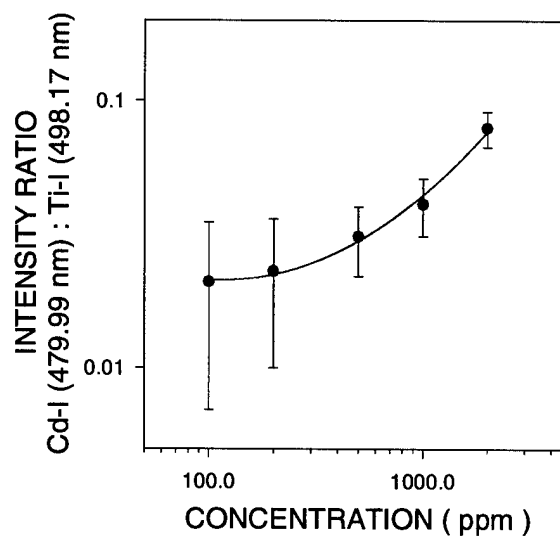
(a) Sand



(b) Silt



(c) Clay



(d) Kaolin

Figure 12: Calibration curves for cadmium (Cd) in (a) sand, (b) silt, (c) clay, and (d) kaolin, based on the intensity ratio of Cd-I (479.99 nm) to Ti-I (498.17 nm).

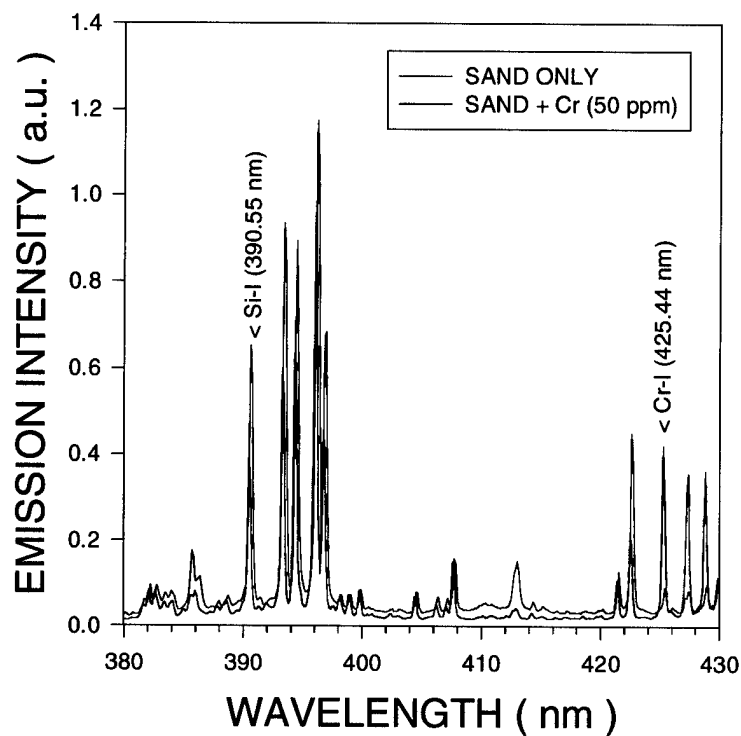


Figure 13: Emission spectrum showing the relevant atomic emission lines of chromium (Cr) and silicon (Si) used in LIBS calibration.

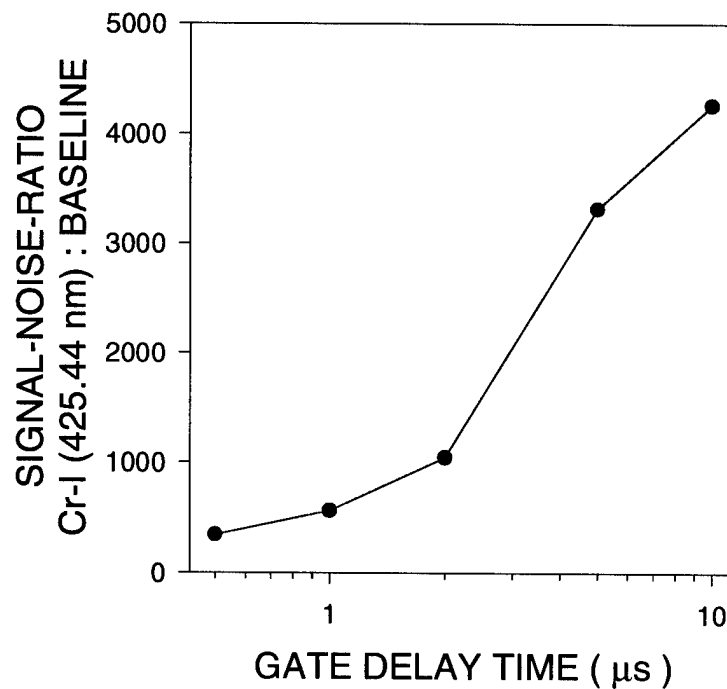
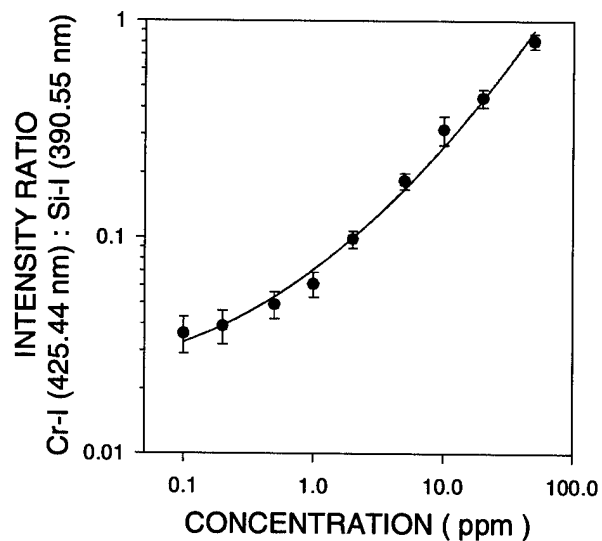
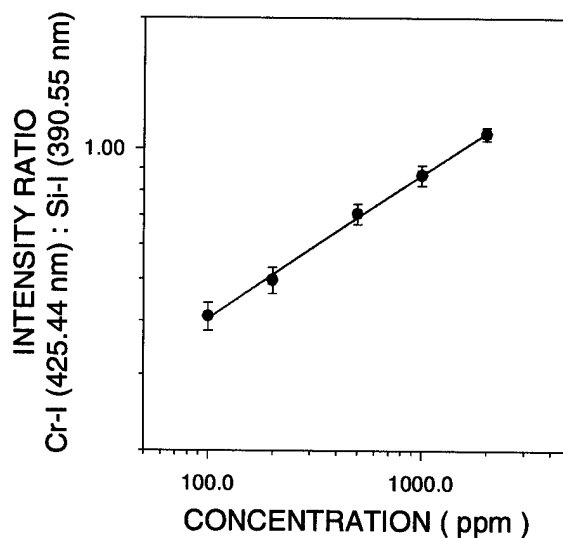


Figure 14: Plot of the signal-noise-ratio of the Cr-I (425.44 nm) line to the background in the vicinity of 417 nm as a function of ICCD gate delay time.

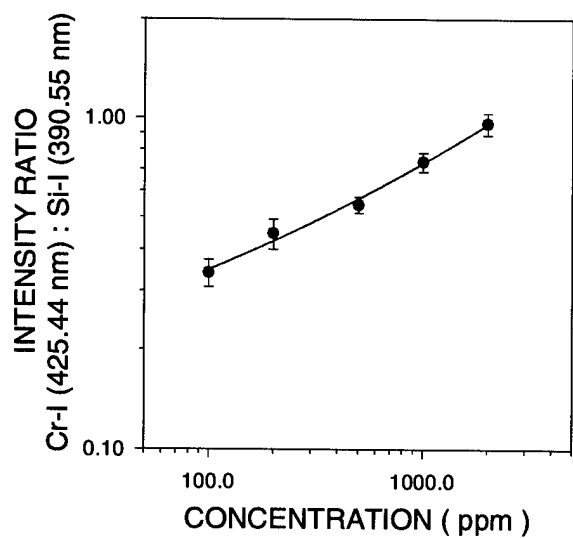
Chromium (Cr)



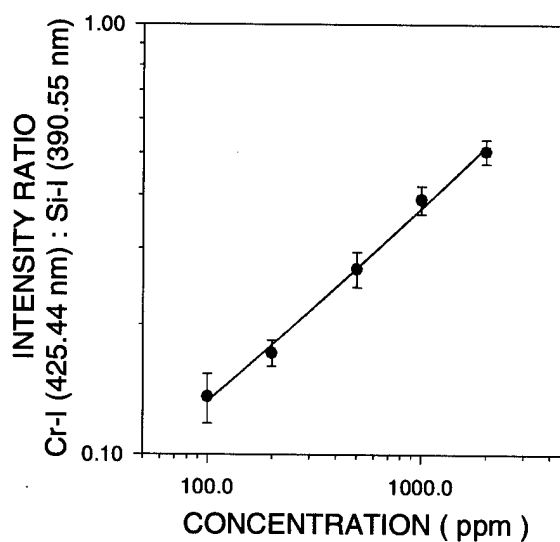
(a) Sand



(b) Silt



(c) Clay



(d) Kaolin

Figure 15: Calibration curves for chromium (Cr) in (a) sand, (b) silt, (c) clay, and (d) kaolin, based on the intensity ratio of Cr-I (425.44 nm) to Si-I (390.55 nm).

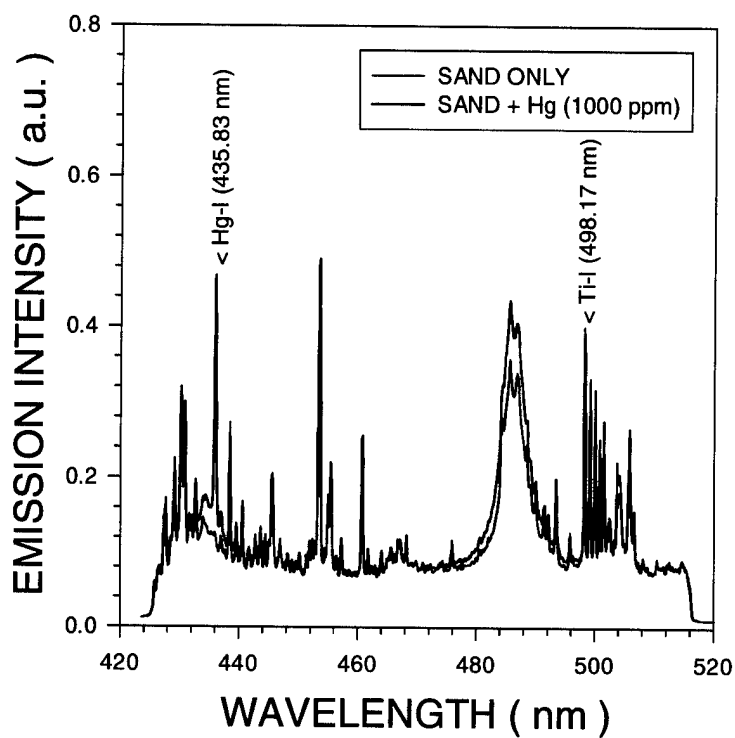


Figure 16: Emission spectrum showing the relevant atomic emission lines of mercury (Hg) and titanium (Ti) used in LIBS calibration.

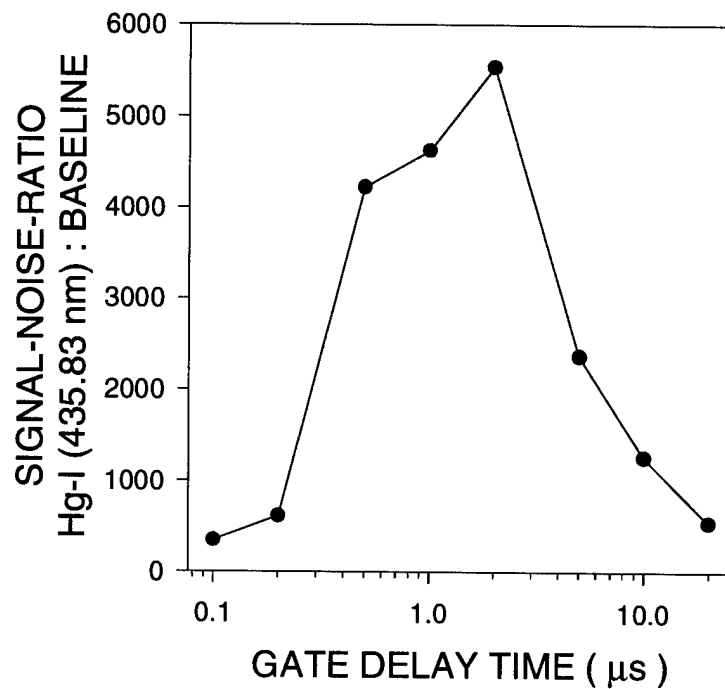
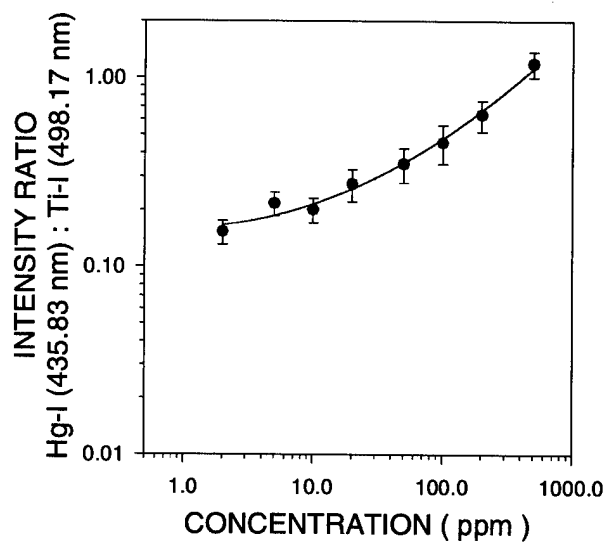
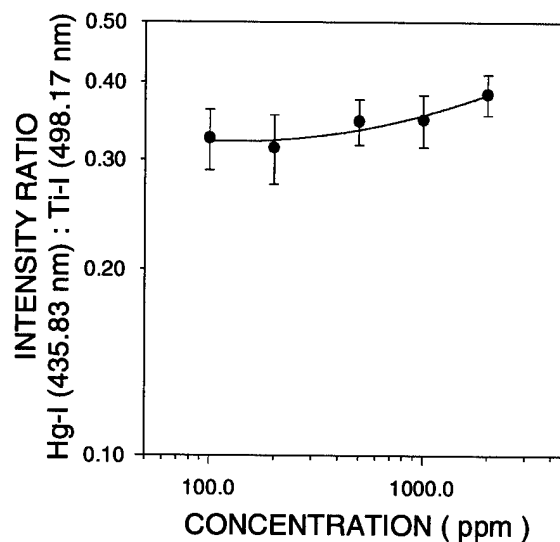


Figure 17: Plot of the signal-noise-ratio of the Hg-I (435.83 nm) line to the background in the vicinity of 460 nm as a function of ICCD gate delay time.

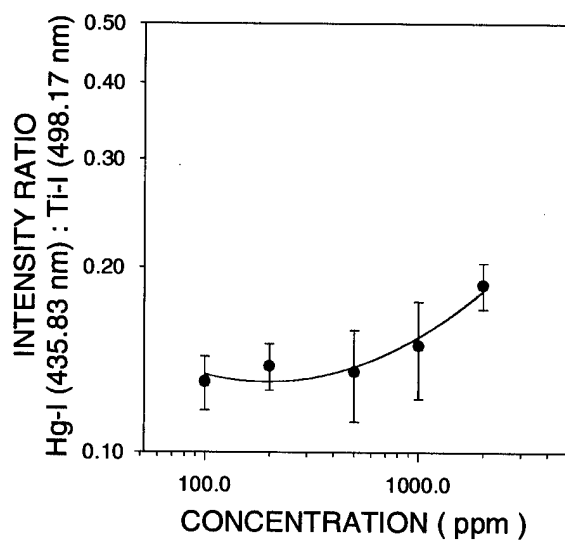
Mercury (Hg)



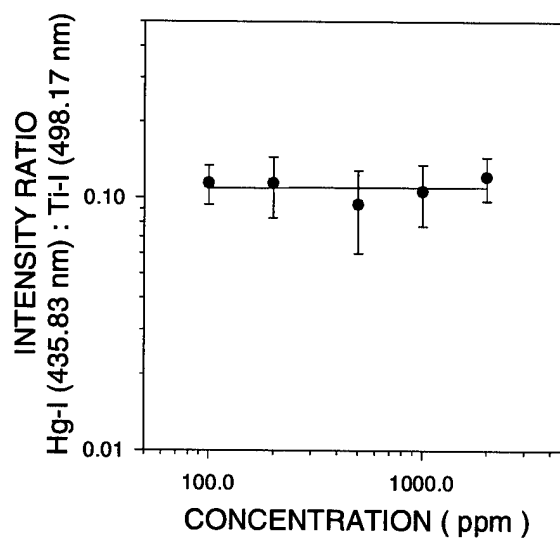
(a) Sand



(b) Silt



(c) Clay



(d) Kaolin

Figure 18: Calibration curves for mercury (Hg) in (a) sand, (b) silt, (c) clay, and (d) kaolin, based on the intensity ratio of Hg-I (435.83 nm) to Ti-I (498.17 nm).

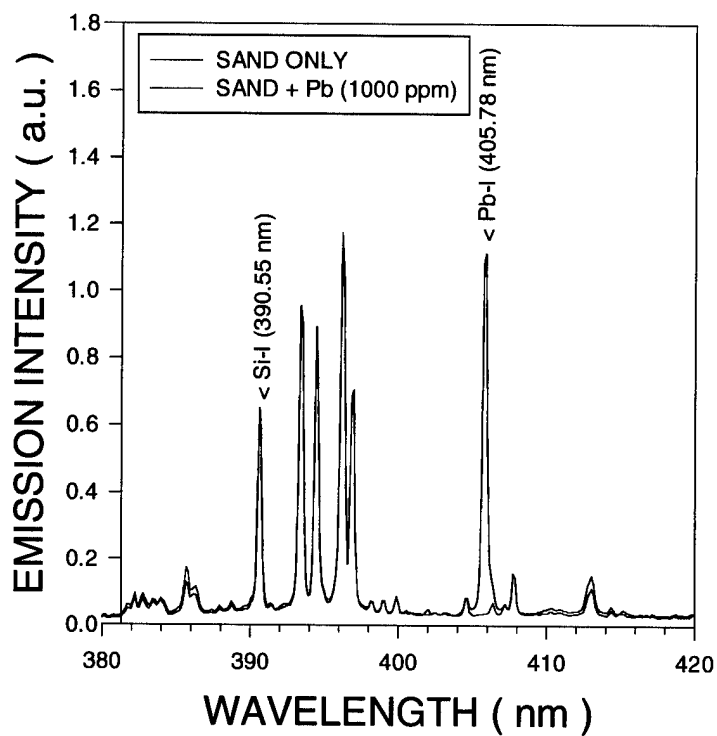


Figure 19: Emission spectrum showing the relevant atomic emission lines of lead (Pb) and silicon (Si) used in LIBS calibration.

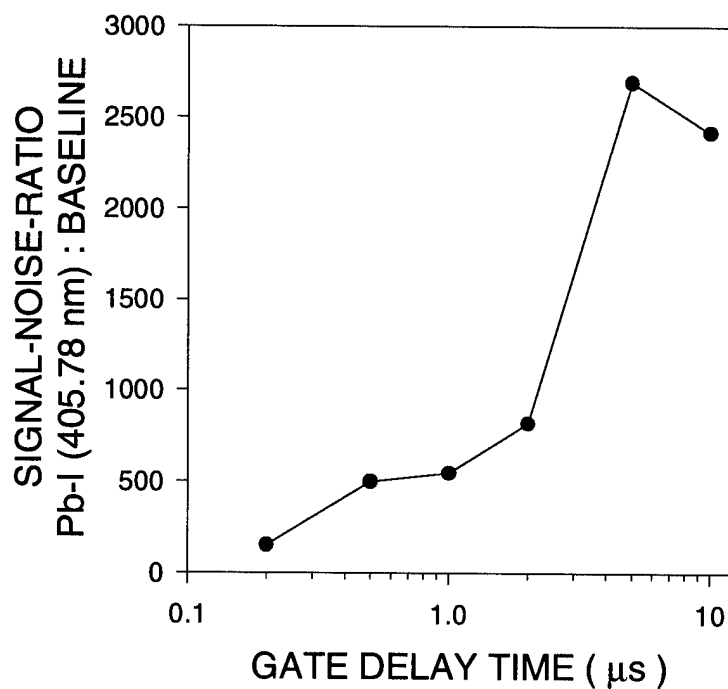
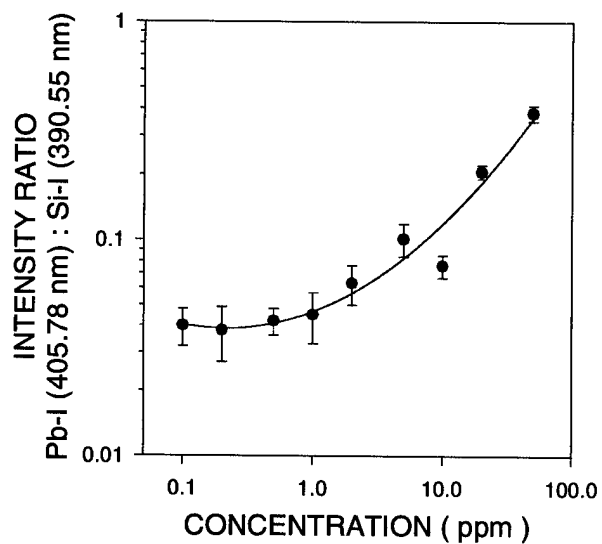
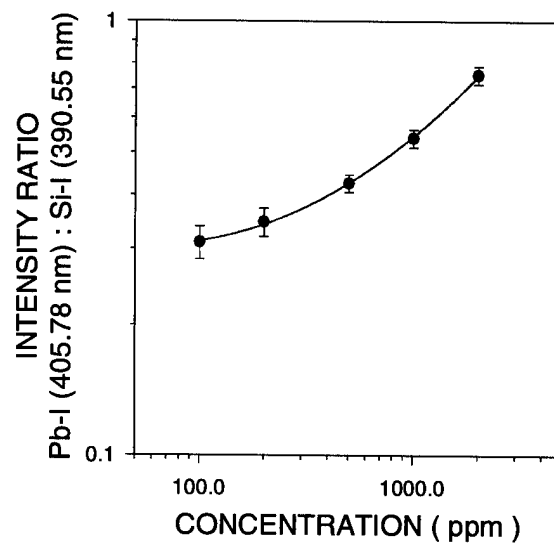


Figure 20: Plot of the signal-noise-ratio of the Pb-I (405.78 nm) line to the background in the vicinity of 409 nm as a function of ICCD gate delay time.

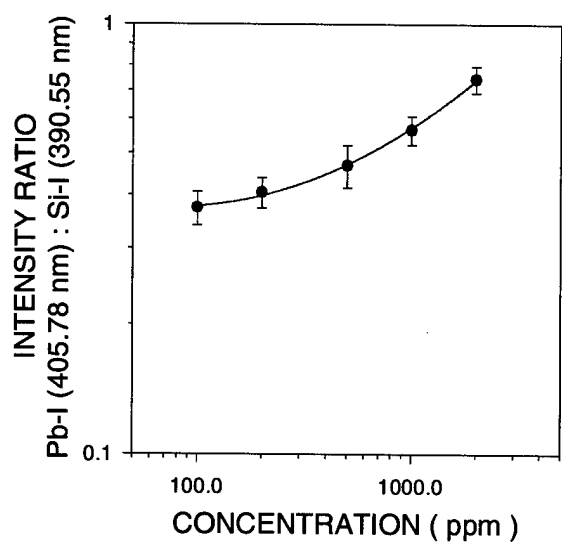
Lead (Pb)



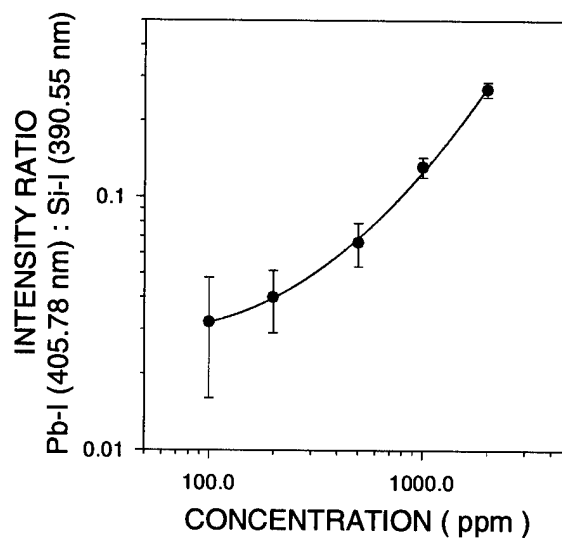
(a) Sand



(b) Silt



(c) Clay



(d) Kaolin

Figure 21: Calibration curves for lead (Pb) in (a) sand, (b) silt, (c) clay, and (d) kaolin, based on the intensity ratio of Pb-I (405.78 nm) to Si-I (390.55 nm).

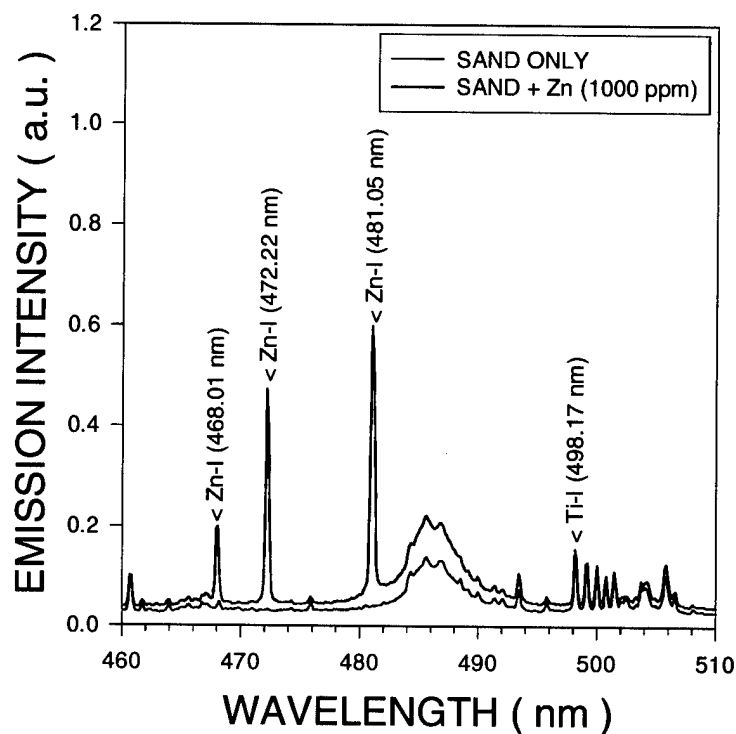


Figure 22: Emission spectrum showing the relevant atomic emission lines of zinc (Zn) and titanium (Ti) used in LIBS calibration.

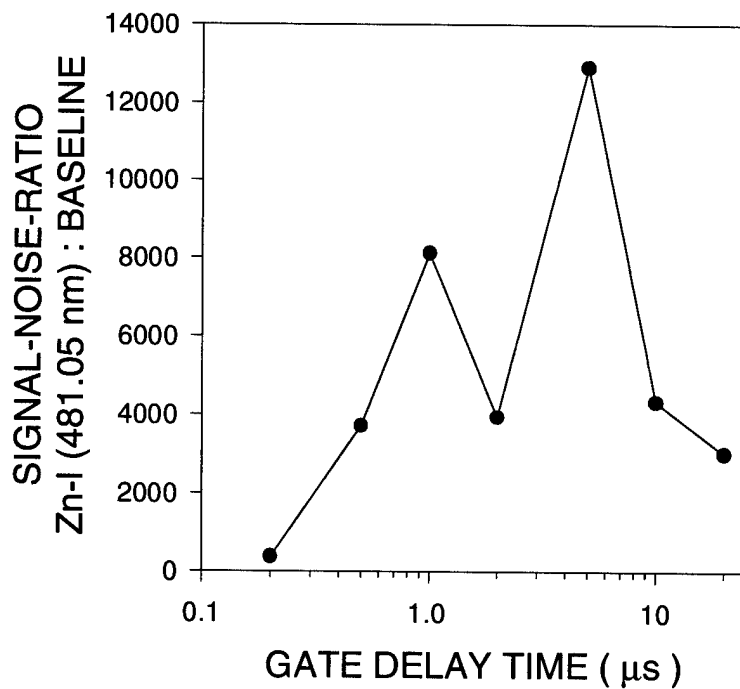
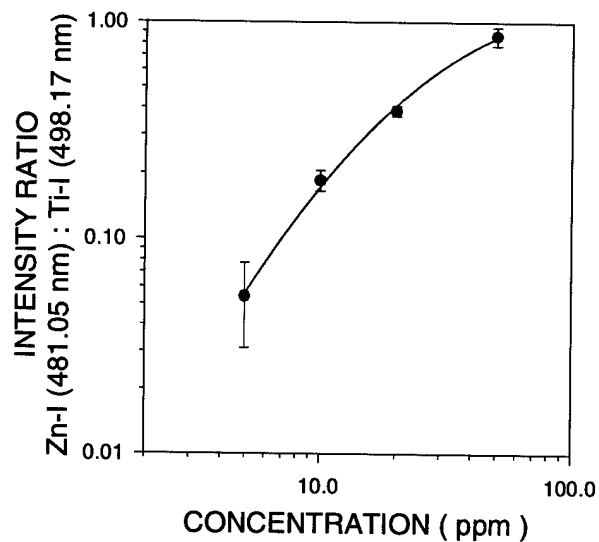
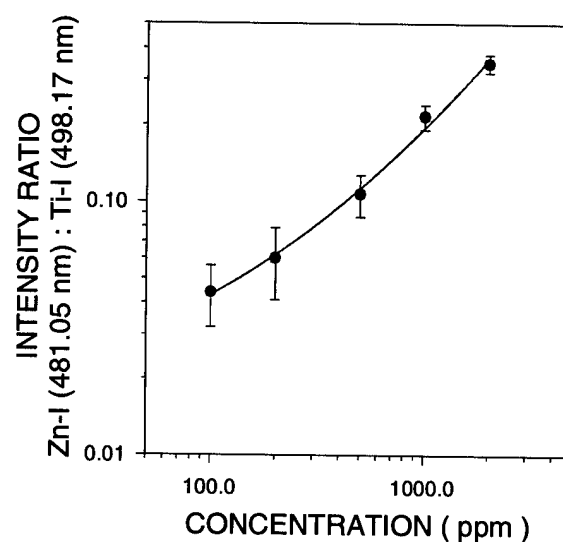


Figure 23: Plot of the signal-noise-ratio of the Zn-I (481.05 nm) line to the background in the vicinity of 479 nm as a function of ICCD gate delay time.

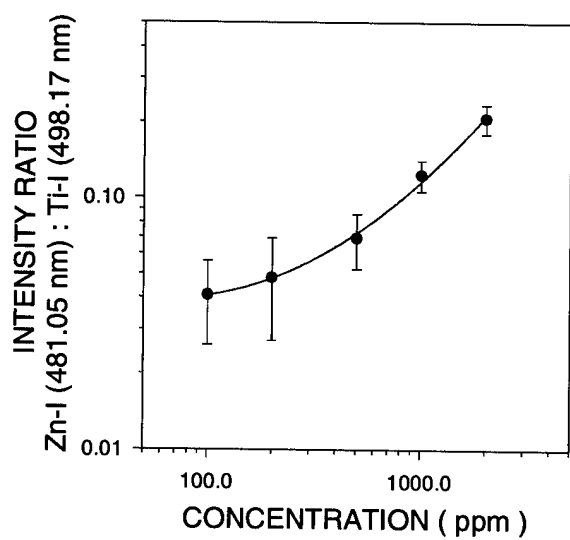
Zinc (Zn)



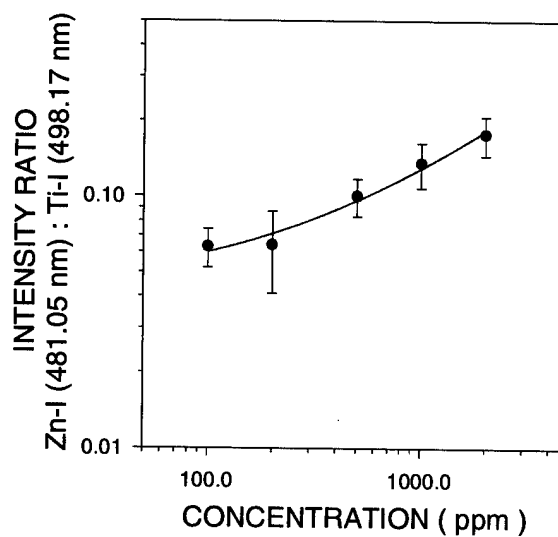
(a) Sand



(b) Silt



(c) Clay



(d) Kaolin

Figure 24: Calibration curves for zinc (Zn) in (a) sand, (b) silt, (c) clay, and (d) kaolin, based on the intensity ratio of Zn-I (481.05 nm) to Ti-I (498.17 nm).

4.4 Detection Limits

Lower detection limits were derived from the calibration data according to the relation

$$C_L = \frac{2S}{M}$$

where

C_L = lower detection limit (concentration),

S = sample standard deviation, and

M = slope of the calibration curve near the lower limit.

Results for each of the heavy metals, in each soil type, are shown in Table 4. Chromium was the most readily detectable element, followed by Pb, Zn, Cd, Hg and with As being the least detectable. It is also evident that detection limits were 1 to 2 orders of magnitude lower in

Table 4: Lower detection limits for As, Cd, Cr, Hg, Pb and Zn in sand, silt, clay and kaolin samples.

Element	Lower Detection Limit (ppm)			
	Sand	Silt	Clay	Kaolin
As	530.	†	†	†
Cd	3.3	160.	360.	830.
Cr	0.42	74.	73.	83.
Hg	11.	1800.	1100.	†
Pb	1.4	150.	210.	340.
Zn	1.6	190.	510.	300.
† - could not be determined from data				

sand than in silt or clays. It has been suggested by Wisbrun *et al.*¹¹ that this is due to the

difference between surface contamination (as in sand) and volume contamination (as in silt and clays). Further investigations are needed to clearly resolve whether surface versus volume contamination is the cause of these differences, or whether chemical reactions (resulting in different chemical bonds) may be affecting the LIBS measurements.

5 Conclusions

Calibration curves have been developed and lower detection limits determined for arsenic, cadmium, chromium, mercury, lead and zinc in sand, silt, clay and kaolin. All six elements were detectable in sand at concentrations approximately two orders of magnitude lower than in silt or clays. These results are in general agreement with work reported by USACE-WES and by Wisbrun *et al.*¹¹

Tests have been performed to demonstrate the variation of LIBS measurements as a function of soil compression and relaxation time. Results indicate that in the application of very accurate LIBS to cone penetrometer systems, one must take into account the time when the analysis is performed, since the LIBS results depend on the relaxation time between compression (cone penetrometer push) and LIBS analysis.

The importance of consistent methods for sample preparation, insuring more homogeneous samples, in LIBS calibration work has been clearly demonstrated. It is unclear whether other LIBS results reported in the literature have followed such careful sample preparation.

No significant variations were found between LIBS measurements performed with an excimer laser and those performed with a Nd:YAG laser for the case of lead in silt.

REFERENCES

1. D.A. Cremers and L.J. Radziemski, "Detection of chlorine and fluorine in air by laser-induced breakdown spectrometry." *Anal. Chem.*, 55, (1983):1252-1256.
2. D.A. Cremers, L.J. Radziemski and T.R. Loree, "Spectrochemical analysis of liquids using the laser spark." *Appl. Spectrosc.*, 38, (1984):721-729.
3. J.R. Wachter and D.A. Cremers, "Determination of uranium in solution using laser-induced breakdown spectroscopy." *Appl. Spectrosc.*, 41, (1987):1042-1048.
4. K.J. Grant, G.L. Paul and J.A. O'Neill, "Quantitative elemental analysis of iron ore by laser-induced breakdown spectroscopy." *Appl. Spectrosc.*, 45, (1991):701-705.
5. L.J. Radziemski, T.R. Loree, D.A. Cremers and N.M. Hoffman, "Time-resolved laser-induced breakdown spectrometry of aerosols." *Anal. Chem.*, 55, (1983):1246-1252.
6. D.K. Ottesen, L.L. Baxter, L.J. Radziemski and J.F. Burrows, "Laser spark emission spectroscopy for in situ, real-time monitoring of pulverized coal particle composition." *Energy & Fuels*, 5, (1991):304-312.
7. W.L. Flower, *et al.*, "A laser-based technique to continuously monitor metal aerosol emissions." *Fuel Proc. Tech.*, 39, (1994):277-284.
8. H.A. Archontaki and S.R. Crouch, "Evaluation of an isolated droplet sample introduction system for laser-induced breakdown spectroscopy." *Appl. Spectrosc.*, 42, (1988):741-746.
9. K.W. Holtzclaw, J. Moore and C.L. Senior, "Real-time optical measurement of alkali species in air for jet engine corrosion testing." *31st Aerospace Sciences Meeting & Exhibit*, Reno, Nevada (1993).
10. D.E. Poulain, and D.R. Alexander, "Laser-induced breakdown spectroscopy of liquid aerosols: droplet salt concentration measurements." *Appl. Spectrosc.*, 49, (1995):569-579.

11. R. Wisbrun, I. Schechter, R. Niessner, H. Schröder and K.L. Kompa, "Detector for trace elemental analysis of solid environmental samples by laser plasma spectroscopy." *Anal. Chem.*, 66, (1994):2964-2975.
12. D.R. Alexander, D.E. Poulain, R.D. Kubik, and M.U. Ahmad, "Automated element identification in laser-induced breakdown spectroscopy studies of contaminated soils." Final Report on U.S. Army Corps of Engineers, Waterways Experiment Station, Contract DACA39-93-K-0052, (1993).
13. D.A. Cremers, J.E. Barefield II, and A.C. Koskelo, "Remote elemental analysis by laser-induced breakdown spectroscopy using a fiber-optic cable." *Appl. Spectrosc.*, 49, (1995):857-860.
14. D.R. Alexander, D.E. Poulain, M.S. Khlif, and E.R. Cespedes, "Influences on detectability of heavy metals in soils by laser-induced breakdown spectroscopy." *IGARSS'96*, Lincoln, Nebraska (27-31 May 1996).